Supporting Information

Out-of-Plane Deformations Determined Mechanics of Vanadium Disulfide (VS_2) Sheets

Guorui Wang[1, 5], Zhepeng Zhang[2], Yanlei Wang[3], Enlai Gao[4], Xiangzheng Jia[4], Zhaohe Dai[1], Chuanxin Weng[1], Luqi Liu[1,*], Yanfeng Zhang[2], Zhong Zhang[1,*]

[1]CAS Key Laboratory of Nanosystem and Hierarchical Fabrication, CAS Center for Excellence in Nanoscience, National Center for Nanoscience and Technology, Beijing, 100190, P.R. China

[2]Department of Materials Science and Engineering, College of Engineering, Peking University, Beijing 100871, People's Republic of China

[3]State Key Laboratory of Multiphase Complex Systems, Beijing Key Laboratory of Ionic Liquids Clean Process, Institute of Process Engineering, Chinese Academy of Sciences, Beijing 100190, China

[4]Department of Engineering Mechanics, School of Civil Engineering, Wuhan University, Wuhan, Hubei 430072, China

[5]Department of Mechanical and Industrial Engineering, University of Toronto, 5 King's College Road, Toronto, Ontario M5S 3G8, Canada

Correspondence and requests for materials should be addressed to L.L. (email: liulq@nanoctr.cn) or to Z.Z. (email: zhong.zhang@nanoctr.cn).

S1. AFM nanoindentation

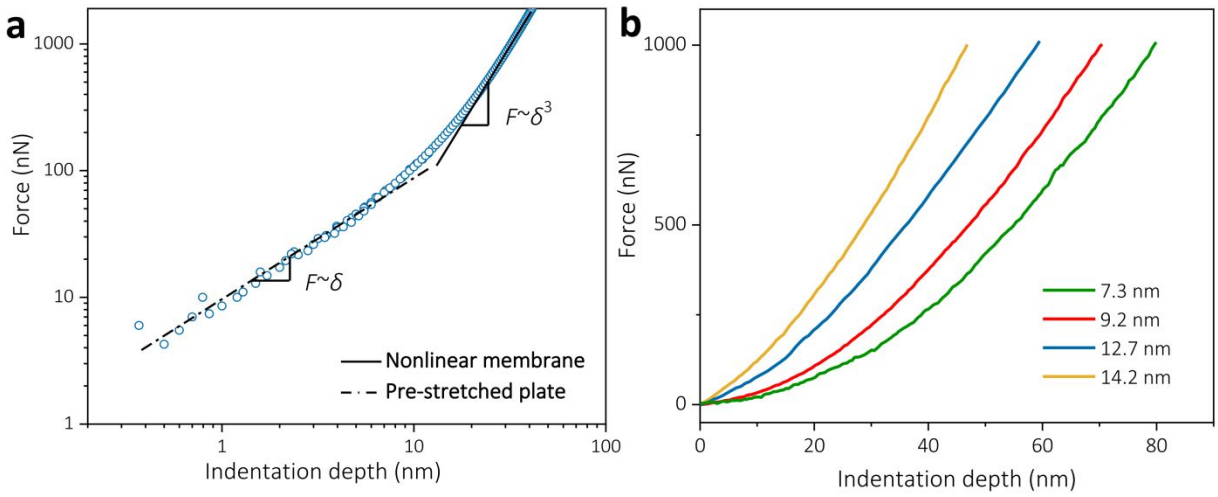

Figure S1. (a) Force-indentation depth curve plotted in logarithmic coordinates, where a linear relationship can be observed in the first stage dominated by pre-tension and bending rigidity, while it gradually becomes a cubic relationship as the force increases with membrane characteristics. (b) Representative force-indentation depth curves for suspended VS_2 nanosheets with different thicknesses.

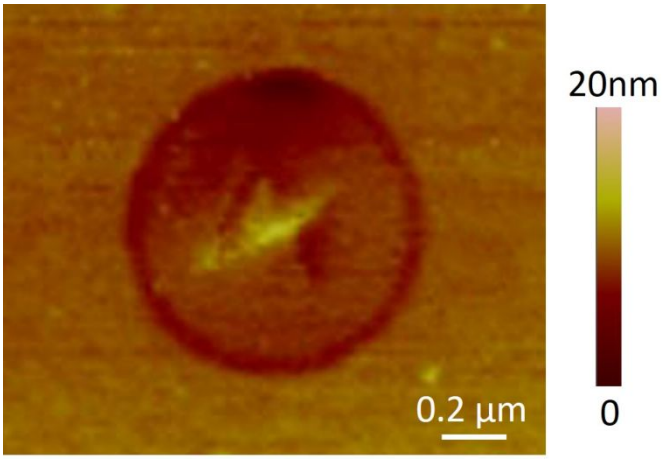

Figure S2. The fracture morphology of VS_2 nanosheet after the nanoindentation test, where a localized crack can be observed.

S2. Lattice parameter of VS_2

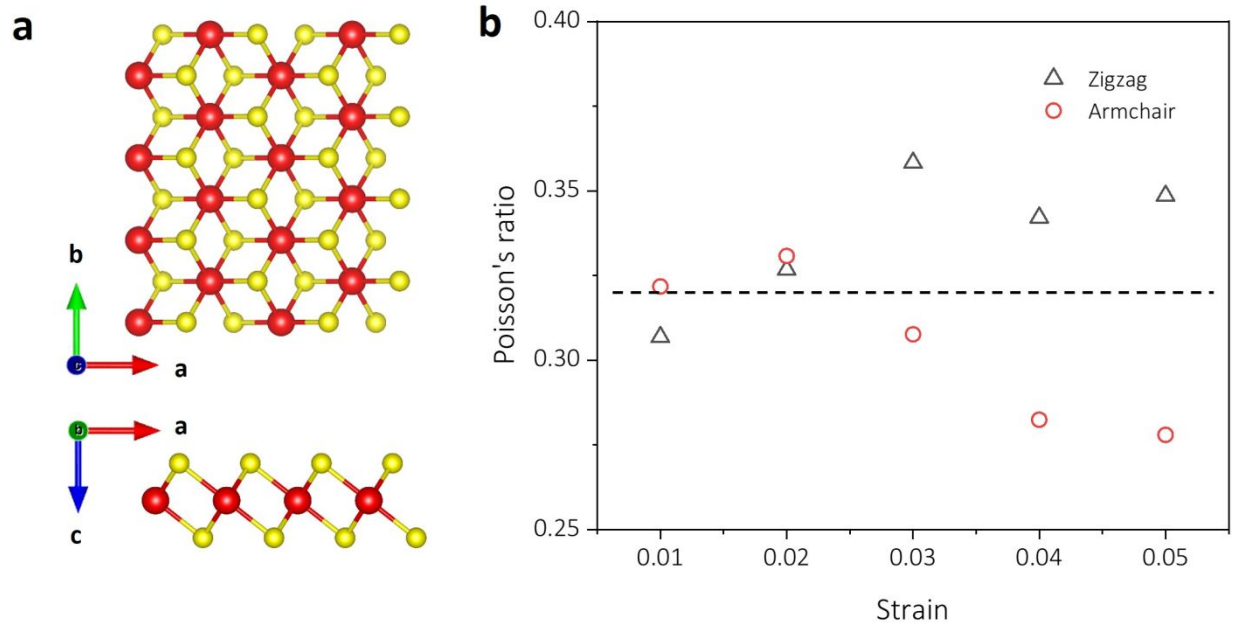

Figure S3. (a) Schematic of atomic configuration of 1T VS_2 used in DFT calculation, where the red atom is vanadium (V) and the yellow atom is sulfur (S). (b) The strain − Poisson's ratio curve of VS_2 in the direction of armchair and zigzag.

Table S1. Parameters for the atomic configuration of VS_2.

$d_{V\text{-}V}$ (Å)	$d_{V\text{-}S}$ (Å)	$Angle_{V\text{-}S\text{-}V}$ (°)	*a* (Å)	*b* (Å)
3.1609	2.35	84.4245	3.1609	5.47087

Table S2. Atomic bond length and angle for different 2D transition metal dichalcogenides materials.

Materials	Bond length (Å)	Bond angle (°)	Ref.
MoS_2	2.31	81.49	[1, 2]
$MoSe_2$	2.51	82.56	[1, 3]
$MoTe_2$	2.70	81.00	[1, 2]
WS_2	2.39	80.80	[1, 4]
VS_2	2.36	84.43 - 85.06	[5, 6]

S3. Geometry of VS_2 buckles

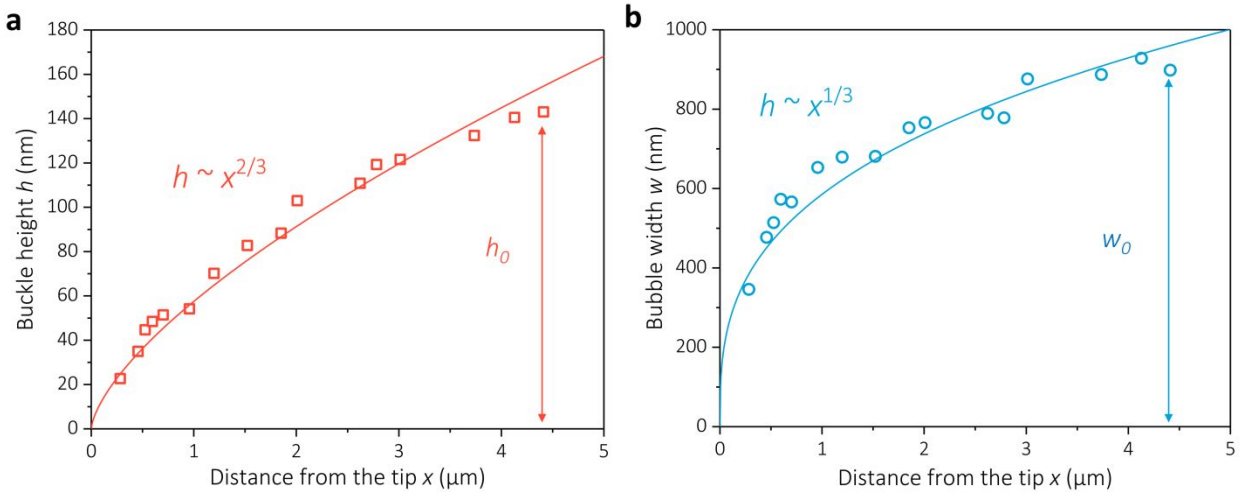

Figure S4. (a) Buckle height and (b) width as a function of the distance from the tip (x). The experimental data are fitted by power functions with 2/3 and 1/3 exponents, respectively.

S4. Bulge test

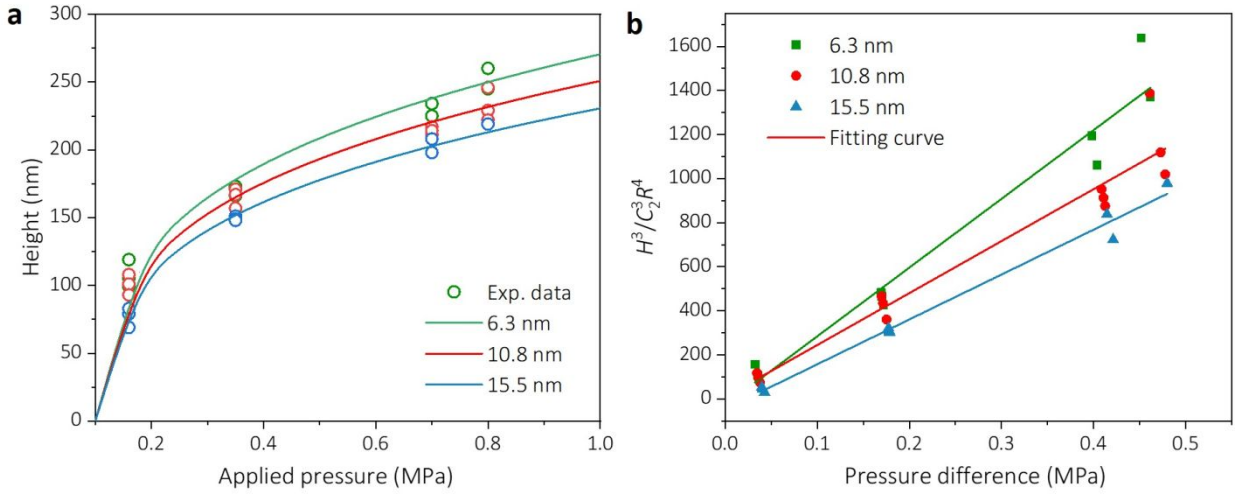

Figure S5. (a) VS_2 bubble height as a function of applied pressure at various thicknesses. (b) Normalized center deflection versus pressure difference for VS_2 bubbles with various thicknesses.

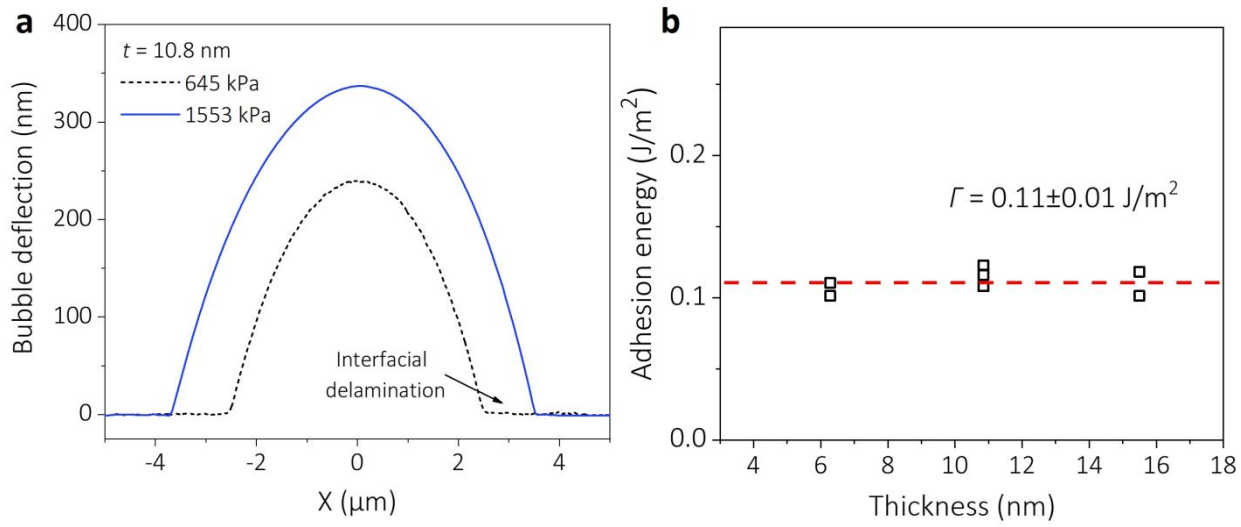

Figure S6. (a) AFM measurement of VS_2 bubble profile after the interfacial delamination. (b) Adhesion energy of VS_2 for different thicknesses.

During the bulging process, the bubble height can be expressed by[7]

$$H = C_2 \sqrt[3]{\frac{\Delta p R^4}{Et}} \tag{S1}$$

where C_2 is a constant as a function of the Poisson's ratio, which is 0.65 for VS_2. Such an H-Δp relationship is further evidenced by our AFM results for VS_2 bubbles with different thicknesses, suggesting the accuracy of measured Young's modulus. Once the delamination occurs, the adhesion energy is derived by seeking minima in the system free energy to achieve an equilibrium configuration:[8, 9]

$$\gamma = \frac{5}{4} C_1 \Delta p H = \frac{5}{4} C_1 \left(\frac{p_0 V_0}{V_0 + V_b} - p_e\right) H \tag{S2}$$

where $C_1 = 0.52$ is a constant depending on the Poisson's ratio, H is the bubble deflection at the center, p_0 is the applied pressure, V_0 is the volume of microcavity, V_b is the bubble volume and p_e is the atmosphere pressure. Based on the AFM measurement of bubble deflection and radius, the adhesion energy can be determined as ~0.11 J/m^2 as shown in Fig. S6b. This agrees well with the recent works reporting the adhesion energy between MoS_2 and Si/SiO_2 substrate (0.082-0.170 J/m^2).[10, 11]

At the critical pressure, the highest strain for a bubble can be obtained by combing Eq. (5), Eq. (S1) and Eq. (S2):

$$\varepsilon_{max} = A(\upsilon) \sqrt{\frac{4\gamma C_2^3}{5 C_1 E t}} \tag{S3}$$

S5. The function *f*(*N*) in two limiting cases

Two limiting cases are taken into account here to elucidate the interlayer shear effect on the bending rigidity. In the case of the perfect bonding between layers, the bending rigidity of multilayers is[12]

$$D_{\text{eff}} = ND_1 + \frac{Et_1{}^3}{12(1-\nu^2)}(N^3 - N) \tag{S4}$$

where D_1=4.87 eV is the calculated bending rigidity of monolayer VS_2. Based on Eq. (S2), we have

$$f(N) = \frac{12D_{eff}(1-\nu^2)}{Et_{total}^3} = 1 - \frac{1}{N^2} + \frac{12(1-\nu^2)D_1}{Et_1{}^3N^2} \tag{S5}$$

where $t_{\text{total}} = Nt_1$ and t_1 is the interlayer distance. For ultra-lubricated layers, the bending rigidity is simply expressed by

$$D_{eff} = ND_1 \tag{S6}$$

and thus

$$f(N) = \frac{12(1-\nu^2)D_1}{Et_1{}^3N^2} \tag{S7}$$

The theoretical limits predicted by Eqs. (S5) and (S7) are plotted as solid lines in Fig. 4g.

Reference

1. Li, J.; Medhekar, N. V.; Shenoy, V. B. Bonding Charge Density and Ultimate Strength of Monolayer Transition Metal Dichalcogenides. *J. Phys. Chem. C* **2013**, *117*, 15842-15848.
2. Kanoun, M. B.; Goumri-Said, S. Tailoring Optoelectronic Properties of Monolayer Transition Metal Dichalcogenide through Alloying. *Materialia* **2020**, *12*, 100708.
3. Wang, W.; Jiang, B.; Qian, C.; Lv, F.; Feng, J.; Zhou, J.; Wang, K.; Yang, C.; Yang, Y.; Guo, S. Pistachio-Shuck-Like MoSe2 /C Core/Shell Nanostructures for High-Performance Potassium-Ion Storage. *Adv. Mater.* **2018**, *30*, 1801812.
4. Bui, V. Q.; Pham, T. T.; Le, D. A.; Thi, C. M.; Le, H. M. A First-principles Investigation of Various Gas (CO, H2O, NO, and O2) Absorptions on a WS2 Monolayer: Stability and Electronic Properties. *J. Phys. Condens. Matter* **2015**, *27*, 305005.
5. Jing, Y.; Zhou, Z.; Cabrera, C. R.; Chen, Z. Metallic VS2 Monolayer: A Promising 2D Anode Material for Lithium Ion Batteries. *J. Phys. Chem. C* **2013**, *117*, 25409-25413.
6. Wang, W.; Sun, Z.; Zhang, W.; Fan, Q.; Sun, Q.; Cui, X.; Xiang, B. First-principles Investigations of Vanadium Disulfide for Lithium and Sodium Ion Battery Applications. *RSC Adv.* **2016**, *6*, 54874-54879.
7. Boddeti, N. G.; Koenig, S. P.; Long, R.; Xiao, J.; Bunch, J. S.; Dunn, M. L. Mechanics of Adhered, Pressurized Graphene Blisters. *J. Appl. Mech.* **2013**, *80*, 040909.
8. Koenig, S. P.; Boddeti, N. G.; Dunn, M. L.; Bunch, J. S. Ultrastrong Adhesion of Graphene Membranes. *Nat. Nanotechnol.* **2011**, *6*, 543-546.
9. Wang, G., Interfacial Friction and Adhesion Between Graphene and Silicon. In *Characterization and Modification of Graphene-Based Interfacial Mechanical Behavior*, Springer: Singapore, 2020; pp 67-96.
10. Sanchez, D. A.; Dai, Z.; Wang, P.; Cantu-Chavez, A.; Brennan, C. J.; Huang, R.; Lu, N. Mechanics of Spontaneously Formed Nanoblisters Trapped by Transferred 2D Crystals. *Proc. Natl. Acad. Sci. USA* **2018**, *115*, 7884-7889.
11. Deng, S.; Gao, E.; Xu, Z.; Berry, V. Adhesion Energy of MoS2 Thin Films on Silicon-Based Substrates Determined via the Attributes of a Single MoS2 Wrinkle. *ACS Appl. Mater. Interfaces* **2017**, *9*, 7812-7818.
12. Gao, W.; Huang, R. Effect of Surface Roughness on Adhesion of Graphene Membranes. *J. Phys. D Appl. Phys.* **2011**, *44*, 452001.